DNS of an unsteady turbulent channel flow driven by a temporary sinusoidal pressure gradient

H. Kawamura and K. Honma
Department of Mechanical Engineering, Science University of Tokyo
Noda-shi, Chiba 278-8510, Japan

Y. Matsuo
National Aerospace Laboratory
Chofu-shi, Tokyo 182-8522, Japan

1 Introduction

With aid of the recent development of computers, various direct numerical simulations(DNS) of turbulence are performed. Although the turbulence itself is unsteady in nature, the mean flow is assumed steady in most of the DNS's. This is because the DNS of the turbulence with an unsteady mean flow requires more computational effort to obtain a stable statistical averaged quantities. In the present study, a temporally sinusoidal pressure gradient is imposed on the turbulent channel flow. The each sinusoidal period is divided into a number of phases and statistical average is obtained for various turbulence quantities.

2 Numerical procedures

The computational domain is given in Fig. 1.

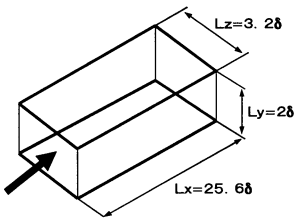

Figure 1: Computational domain

The fundamental equations are
the continuity equation :

$$\frac{\partial u_i^+}{\partial x_i^*} = 0. \qquad (1)$$

and the momentum equation :

$$\frac{\partial u_i^+}{\partial t^+} + u_j^+ \frac{\partial u_i^+}{\partial x_j^*} = -\frac{\partial p^+}{\partial x_j^*} + \frac{1}{Re_{\tau s}} \frac{\partial^2 u_i^+}{\partial x_j^{*2}} + P_x^+. \qquad (2)$$

The sinusoidal pressure gradient is specified as

$$P_x^+ = A sin \frac{2\pi}{T^+} t^+ + 1.0, \qquad (3)$$

where the variables are normalized by channel half width δ and the friction velocity $u_{\tau s}$ for the steady state; that is, A=0. The constant value of 1.0 corresponds to the steady pressure gradient with A=0. The amplitude A has been set to 6.0. This selection is rather arbitrary. It causes the flow rate to oscillate about $\pm$ 50 % around a mean value. The time of one cycle T^+ is 6.0, which is so selected that an unsteady effect appears while flow reversal does not take place. The Reynolds number for A=0 is $Re_{\tau s}$ = 180, which is the value often simulated since the first DNS by Kim et al (1987).

The propagation speed of pressure, is assumed to be enough large so that the mean pressure gradient is uniform in the whole channel and thus the flow is assumed to be fully developed in the streamwise direction. The mean flow is in x direction. The periodic boundary condition is applied in x and z directions. The computational conditions are given in Table 1. The discretization scheme was a so-called 'consistent scheme' by Kawamura (1995), in which a special attention is paid for the consistency between the analytical and the numerical differentiations so that not only the momentum but also the kinetic energy can be well preserved.

3 Results

3.1 Mean velocity profiles

Fig. 2 shows the variation of the pressure gradient. One cycle is divided into 16 phases. The turbulence quantities are averaged within each phase over 15 cycles. The mean velocity, which is averaged over the channel section, is given also in Fig. 2. Its maximum and minimum points are shifted from those of the pressure gradient. The mean velocity increases for the positive pressure gradient, it decreases for the negative pressure gradient. The variation of the ensemble averaged velocity profile is shown in Figs. 3 and 4.

The velocity in Fig. 3 is normalized by $u_{\tau s}$.

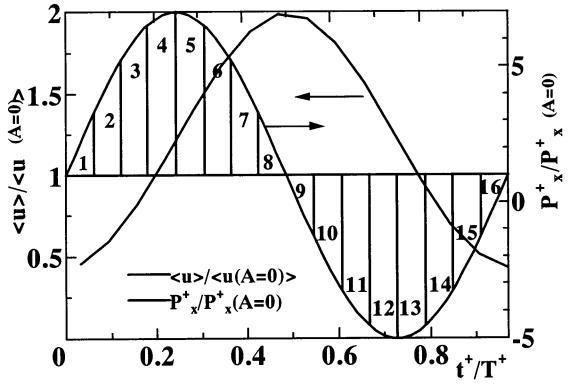

Figure 2: Change of pressure gradient and bulk mean velocity

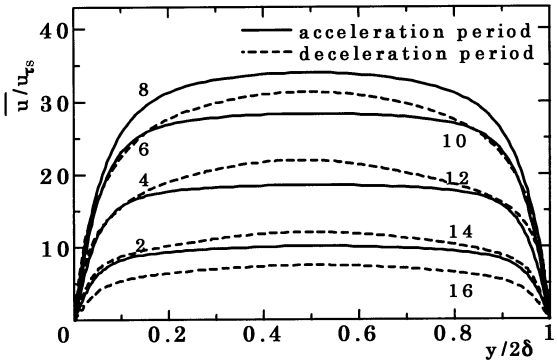

Figure 3: Mean-velocity profiles normalized by $u_{\tau s}$

The velocity in Fig. 4 is normalized by the instantaneous friction velocity $u_{\tau *}$. In the acceleration phase, the profiles are flattened in the channel center, while it is more peaked in the deceleration one. The mean velocity averaged over one cycle is also

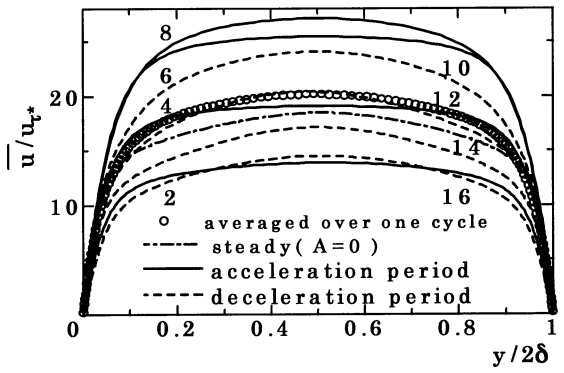

Figure 4: Mean-velocity profiles normalized by $u_{\tau *}$

given in Fig. 4. It is rather larger than the steady state one (A=0). This indicates that the present oscillatory pressure drop results in a higher total flow rate than the steady state one for the same time averaged pressure gradient. The mean velocity is replotted in the semi-logarithmic coordinates in Fig. 5. The mean velocity in this plot is mostly larger than the well-known steady state logarithmic distribution, which suggests a kind of "laminarization" takes place.

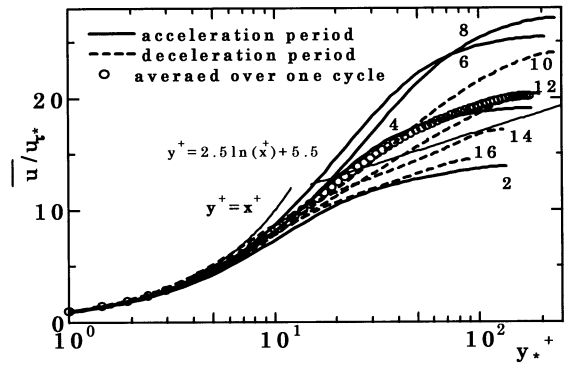

Figure 5: Mean-velocity profiles normalized by $u_{\tau *}$

The friction coefficient :

$$C_f = 2\tau_w/\rho\overline{u_m}^2 \qquad (4)$$

is shown versus the instantaneous Reynolds number $Re_m = \overline{u_m}2\delta/\nu$ in Fig. 6. The plots draw a circle around the steady state correlation given by Dean (1978) : C_f=$0.073Re_m^{-1/4}$. The friction coefficient is larger than the steady state correlation in the early period of the acceleration (phase 1-2), while it is smaller in most of the period. The dependence of C_f upon Re_m is more pronounced than in the steady state.

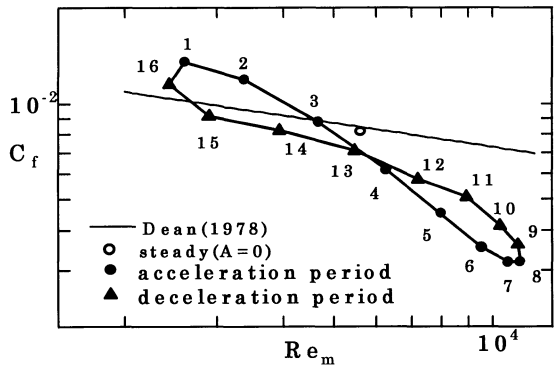

Figure 6: Dependence of wall shear stress on Reynolds number

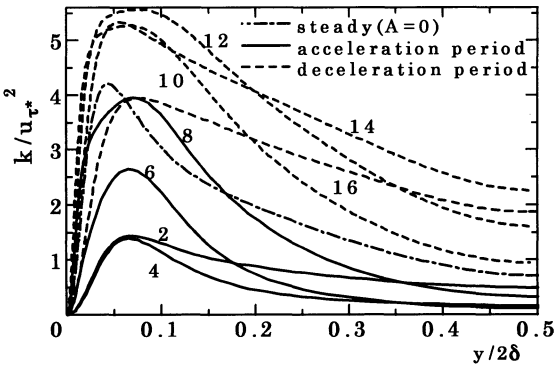

Figure 8: Turbulent kinetic energy normalized by $u_{\tau*}{}^2$

3.2 Turbulent kinetic energy

The distribution of the turbulence energy normalized by $u_{\tau s}$ is given in Fig. 7. It is very much different from the one for the steady state. The turbulence energy is larger than the steady state one when the pressure gradient is decreasing (phases 8-13), while it is smaller when increasing (phases 14-15). The peak of the turbulence energy arises away from the wall compared in the steady state in both acceleration and deceleration periods.

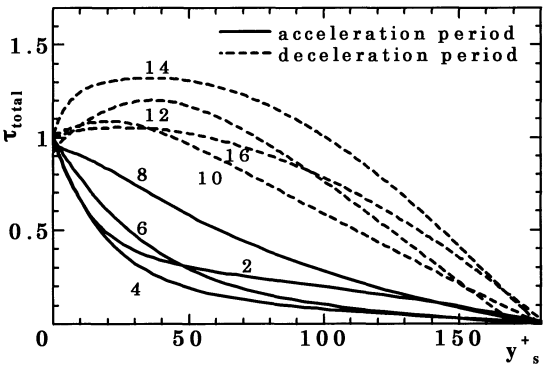

Figure 9: Total shear stress normalized by $u_{\tau*}{}^2$

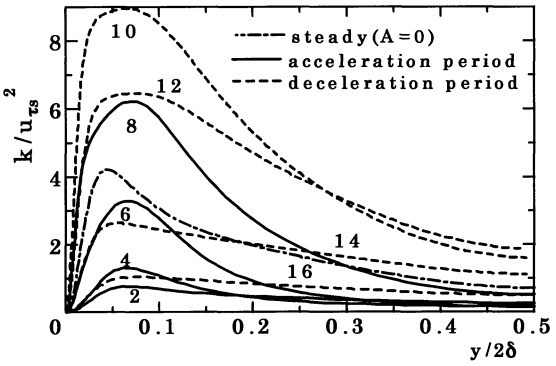

Figure 7: Turbulent kinetic energy normalized by $u_{\tau s}{}^2$

Next, the turbulence energy normalized by the instantaneous friction velocity $u_{\tau*}{}^2$ is shown in Fig. 8. In this case, the normalized k is larger than the steady state one in the deceleration period (phase 8-16), while smaller in the acceleration one (phase 1-6).

To examine the above points, the total shear stress is shown in Fig. 9. In the acceleration period, the total shear stress is decreased. The averaged momentum equation can be expressed as

$$\frac{\partial \overline{u}}{\partial t} = -\frac{1}{\rho}\frac{\partial \overline{p}}{\partial x} + \frac{\partial}{\partial y}(\nu \frac{\partial \overline{u}}{\partial y} - \overline{u'v'}). \quad (5)$$

When the above equation is integrated from $y = 0$ to $y = y$, it becomes

$$\int_0^y \frac{\partial \overline{u}}{\partial t} dy = -\int_0^y \frac{1}{\rho}\frac{\partial \overline{p}}{\partial x} dy + [\ \nu \frac{\partial \overline{u}}{\partial y} - \overline{u'v'}\ ]_0^y. \quad (6)$$

Thus, the total shear stress normalized by the instantaneous friction velocity $u_{\tau*}{}^2$, can be obtained as

$$\tau_{total}/\rho {u_{\tau*}}^2 = -\overline{u_*^{+\prime} v_*^{+\prime}} + \frac{\overline{du_*^+}}{dy_*^+} \quad (7)$$

$$= 1 - 1/Re_{\tau*}(P^+_{x*} y^+_* - \int_0^{y^+_*} \frac{\overline{du_*^+}}{dt_*^+} dy^+_*) \quad (8)$$

In the acceleration period, velocity-gradient term ${P_{x*}}^+$ becomes large; on the other hand, the acceleration term $\int_0^{y_*^+} \frac{du_*^+}{dt_*^+} dy_*^+$ is small in the wall vicinity because the velocity itself is small. Thus the gradient of the total shear stress exhibits a large negative value in the wall vicinity. The Reynolds shear

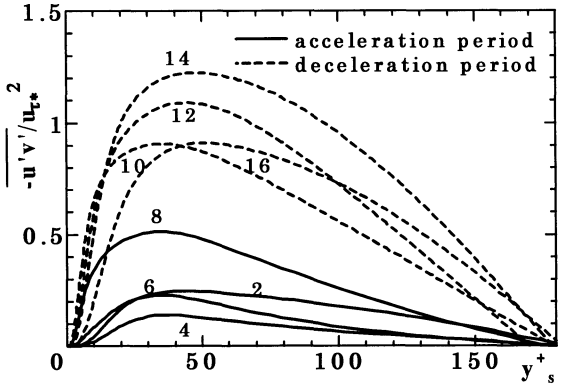

Figure 10: Reynolds shear stress normalized by ${u_{\tau*}}^2$

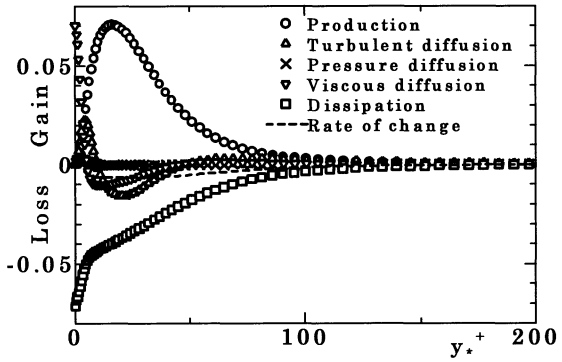

Figure 11: Budget of turbulent kinetic energy in the acceleration period (phase 6)

stress is shown in Fig. 10. It suppressed is in the acceleration period. This is because the total shear stress itself is decreased in the acceleration period as discussed above.

The budget of the turbulent energy is shown in Figs. 11-14. In the acceleration period, the peak of the production is much smaller than its steady state value of 0.25. This is because the Reynolds shear stress is decreased as seen in Fig. 10. These indicate that, in the acceleration phase, a phenomena similar to the "laminarization" takes place and thus the turbulent energy is decreased. In the deceleration period, on the other hand, the pressure gradient term ${P_{x*}}^+$ becomes negative, so the Reynolds shear stress increases remarkably. In consequence, the production term and the turbulent kinetic energy are increased.

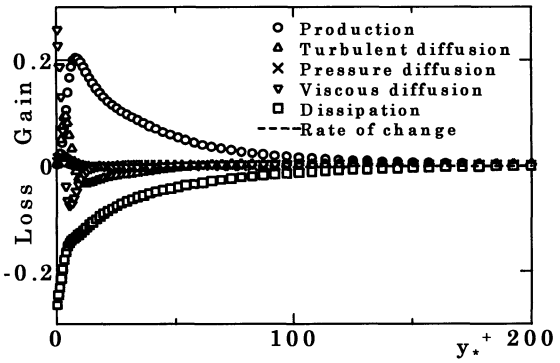

Figure 12: Budget of turbulent kinetic energy in the acceleration period (phase 8)

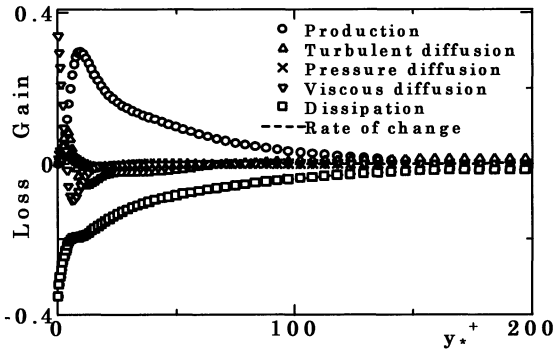

Figure 13: Budget of turbulent kinetic energy in the deceleration period (phase 12)

3.3 Visualization of the turbulence structure

Instantaneous high and low velocity regions are shown for Figs. 15 and 16 in acceleration and deceleration periods, respectively. In the accelera-

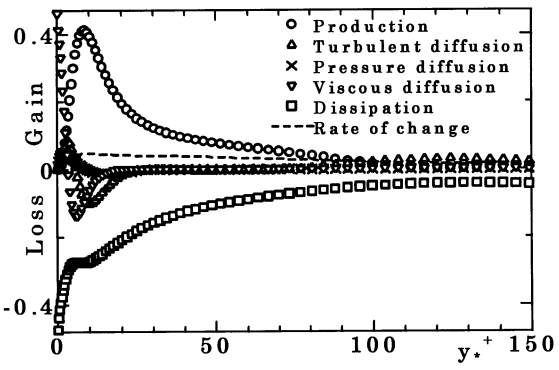

Figure 14: Budget of turbulent kinetic energy in the deceleration period (phase 14)

tion period, the high and low speed streaks are very much elongated. They are connected from upstream to downstream boundaries. The time instance illustrated in Fig. 15 roughly corresponds to the peak of the pressure gradient. It's interesting to see that wary fractured low pressure regions start to propagate from the upstream region.

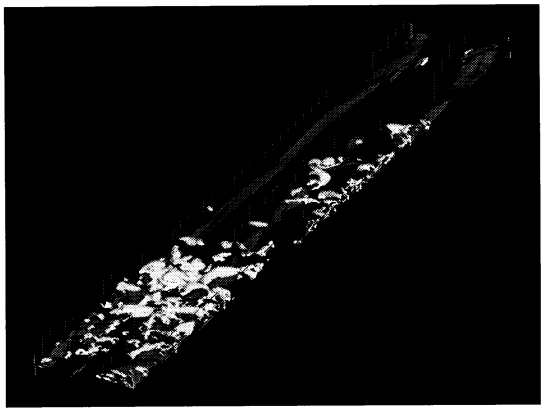

Figure 15: High and low speed streaks in acceleration period. white: p'^{+} <-3.0, dark-gray: u'^{+} >3.0, light-gray: u'^{+} <-3.0 (phase 4-5)

On the other hand, in the deceleration period, the structures are fractured into complex segments. The streaky structures are still observed, but it is elongated in the spanwise direction. Moreover many ramped structures appear not only in the wall vicinity but also in the central region.

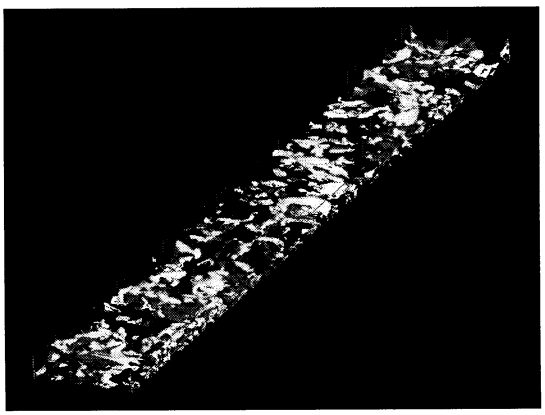

Figure 16: High and low speed streaks in deceleration period. white: p'^{+} <-3.0, dark-gray: u'^{+} >3.0, light-gray: u'^{+} <-3.0 (phase 10-11)

The streamwise vorticity fluctuations are shown in Figs. 17 and 18. In the acceleration period, the vorticity fluctuations like the elongated streaky structure seen in Fig. 15 are not observed.

On the other hand, in the deceleration period, the vorticity fluctuations are elongated in the spanwise direction. Further study is required in conjunction with the vortex dynamics.

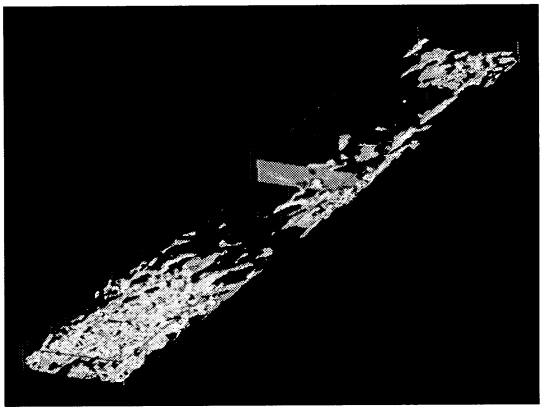

Figure 17: The streamwise vorticity fluctuations in the acceleration period. white: $w_x'^{+}$ <-0.2, dark gray to light gray: $w_x'^{+}$=-0.2 to 0.2 (phase 4-5)

3.4 Two-point correlation

To examine the adequacy of the computational domain, two-point correlations in the streamwise

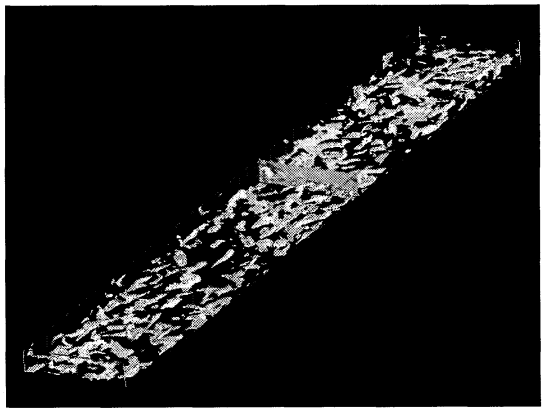

Figure 18: The streamwise vorticity fluctuations in the deceleration period. white: $w_x'^+$ <-0.2, dark gray to light gray: $w_x'^+$=-0.2 to 0.2 (phase 10-11)

direction at two y-locations, one very close to the wall and the other close to the centerline, are shown in Figs. 19 and 20. It indicates that they nearly fall off to zero in the channel center (Fig. 19), but not in the acceleration phase in the wall vicinity (Fig. 20). In this respect the streamwise domain is still not enough large to apply the periodic boundary condition for some of the phases.

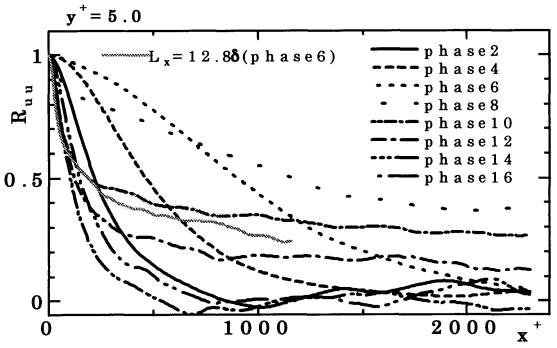

Figure 19: Two-point correlations in x direction

4 Nomenclature

p^+ $= p/\rho {u_{\tau s}}^2$
p_*^+ $= p/\rho {u_{\tau *}}^2$
$Re_{\tau s}$; Reynolds number of steady state $= u_{\tau s}\delta/\nu$
$Re_{\tau *}$; instantaneous Reynolds number $= u_{\tau *}\delta/\nu$
t^+ $= u_{\tau s}t/\delta$
t_*^+ $= u_{\tau *}t/\delta$
u^+ $= u/u_{\tau s}$

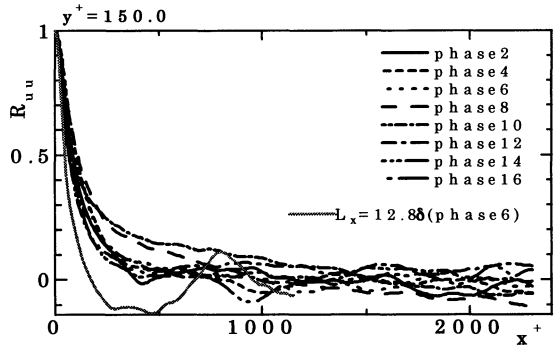

Figure 20: Two-point correlations in x direction

Table 1: Computational conditions

Grid		Staggered grid
Coupling algorithm		Fractional step method
Time advancement	Viscous term(y)	Crank-Nicolson method
	Other	Adams-Bashforth method
Scheme	Convective term	2^{nd}-Consistent
	Viscous term	2^{nd}-Central
Boundary condition		Periodic(x, z direction), Non-slip (y direction)
Grid number		$512 \times 128 \times 128$
Computation volume ($L_x \times L_y \times L_z$)		$25.6\delta \times 2\delta \times 3.2\delta$
Visualization volume		$25.6\delta \times \delta \times 3.2\delta$
The grid spacing		$\Delta x^+ = 9.0, \Delta z^+ = 4.5$, $\Delta y^+ = 0.2 \sim 5.75$
Reynolds number		$Re_{\tau s} = 180$

u_s^+ $= u/u_{\tau s}$
u_*^+ $= u/u_{\tau *}$
$u_{\tau s}$; friction velocity at steady state(A=0)
$u_{\tau *}$; instantaneous friction velocity
x_i^* $= x_i/\delta$
y^+ $= u_{\tau s}y/\nu$
y_*^+ $= u_{\tau *}y/\nu$
$< >$; avereged over channel section

5 References

Dean, R.B., 1978, Journal of Fluids Engineering, Vol.100, pp.215-222.

Kawamura, H., 1995, in: The Recent Developments in Turbulence Research. International Academic Publishers, pp.54-60.

Kim, J. et.al., 1987, Journal of Fluid Mechanics, Vol.177, pp. 133-166.